

Facile Electrodeposition and Corrosion Properties of Zirconium-based Superhydrophobic Thin Films on Aluminum

R. FARID¹, D.K. SARKAR^{1,*} AND D. DE²

¹*University Research Centre on Aluminium (CURAL) and Aluminium Research Centre-REGAL, University of Québec at Chicoutimi (UQAC), 555 Boulevard de l'Université, Chicoutimi, Québec, G7H 2B1, Canada*
²*Energy Institute, Bangalore (a unit of R.G.I.P.T), Muddenahalli, Chickkabalapura, Karnataka 562101, India*

The development of corrosion resistant superhydrophobic thin films on aluminum surfaces has attracted great interest for industrial applications. In the present work, zirconium-based superhydrophobic thin films were fabricated on AA6061 aluminum alloy substrates by a simple electrodeposition process. The thin film coated Al substrate exhibited excellent superhydrophobicity with a higher water contact angle of $162 \pm 3^\circ$ compared to the hydrophilic as-received Al substrate with a contact angle of $83 \pm 2^\circ$. The surface morphology of the fabricated thin films on Al substrate shows uniform micro-nano porous structures. The polarization resistance of the as-received Al and the zirconium-based superhydrophobic thin films on the Al substrate are $23 \text{ k}\Omega\cdot\text{cm}^2$ and $788 \text{ k}\Omega\cdot\text{cm}^2$, respectively. These results show excellent anti-corrosion property of zirconium-based superhydrophobic thin films to provide high corrosion protection for Al substrates.

Keywords: Aluminum, electrodeposition, superhydrophobic surface, potentiodynamic polarization, corrosion resistance

1 INTRODUCTION

Superhydrophobic surfaces are characterized by apparent water contact angle greater than 150° and low contact angle hysteresis [1]. Inspired by nature,

*Corresponding author: e-mail: dsarkar@uqac.ca

studies reveal that the combination of surface roughness and low surface energy material can realize superhydrophobicity [2,3]. Nowadays, superhydrophobic surfaces attract a great deal of interest in various fields of applications due to their self-cleaning, anti-corrosion, anti-icing, and oil-water separation properties [4–7].

Aluminum (Al) alloys have attracted high interest in many applications due to their high strength, low cost and high-performance [8], these materials are used in aerospace, automobile, aircraft, boats, electronic industries, etc. [9,10]. Despite their good properties, Al alloys show weak resistance to corrosion in marine environments resulting from the penetration of chloride ions to the protective oxide film formed on alumina [11,12], which limits their applications. One of the current industrial strategies to protect metals against corrosion by applying superhydrophobic coatings with self-cleaning properties. Such coating provides excellent anti-corrosion properties to protect metal surfaces, especially for Al and its alloys. In that regard, many researchers reported the effect of superhydrophobic protective thin films on the Al surfaces [13-16]. Huang *et al.* [14] reported the synthesis of superhydrophobic thin films on Al alloy substrates, with good corrosion resistance properties, using chemical etching by nitric acid, and an ethanolic stearic acid solution was used for passivation. In another study, Li *et al.* [15] reported the fabrication of superhydrophobic Al surface with a water contact angle of 155.7° using hydrochloric acid followed by potassium permanganate passivation and modification by fluoroalkyl-silane. The surface morphology of the samples showed hierarchical terrace-like structures and a nano-scale coral-like network of bulge structures. The superhydrophobic behavior of the surfaces was due to nano-microstructural morphology and its low surface energy [16].

A number of materials were used in our group, in the fabrication of superhydrophobic thin films for the corrosion protection of Al alloys, such as cobalt, zinc, copper, and nickel [17–21]. Zirconium is also an effective material for the corrosion protection of Al. The zirconium-based materials have attracted great interest due to their good mechanical strength, thermal stability as well as the strong alkali and acid resistant property compared to other ceramic materials [22]. In this regard, many research works were reported on the fabrication of Zr-based superhydrophobic thin films on different substrates used for various applications. Fan *et al.* [23] reported the fabrication of the Zr-based superhydrophobic thin films via electrodeposition process on carbon fiber fabrics for the separation of the water-oil mixture. Indraneel and Goutam [24] reported the fabrication of Zr-based superhydrophobic thin films on the cotton fabrics. In their work, the superhydrophobic thin films were synthesized by the immersion of dried cotton fabrics in homogenized fluorinated silyl-functionalized zirconia solution. They have reported that the coated fabrics show good washing durability, water repellency, and self-cleaning ability.

Although zirconium-based materials have several applications, studies on the corrosion protection of Al by zirconium-based materials are less reported. As far as corrosion studies on the Zr-based thin films are concern, typically,

they are hydrophilic in nature and applied on different metals. Haibin *et al.* [25] reported the use of Zr-based thin films for the corrosion protection of mild steel. In their work, they have deposited Zr-based hydrophilic thin films on flat sheets of mild steel by dip coating process. They have reported that the polarization resistance of the Zr-based thin films was $299 \Omega \cdot \text{cm}^2$ as compared to $40 \Omega \cdot \text{cm}^2$ for as-received steel substrates in 1 M HCl solution. Li *et al.* [26] studied the corrosion properties of the Zr-based conversion thin films on Al substrates. They have reported a polarization resistance of $47 \text{ k}\Omega \cdot \text{cm}^2$ for the Zr-based thin films compared to $13 \text{ k}\Omega \cdot \text{cm}^2$ for as-received Al substrate.

On the other hand, there have been few works on the corrosion study of zirconium-based superhydrophobic thin films, such as the work done by Chen *et al.* [2] where they fabricate superhydrophobic palmitate film on steel substrates. They reported a corrosion current density (I_{corr}) of $19.5 \mu\text{A}/\text{cm}^2$ for the steel substrate compared to $0.92 \mu\text{A}/\text{cm}^2$ for the superhydrophobic palmitate film. The decrease in I_{corr} values indicates the better corrosion protection provided by the superhydrophobic thin film.

In this work, Zirconium-based thin films were successfully fabricated by one step electrochemical process on Al substrates. The morphology, chemical composition, wettability, and corrosion behavior of the synthesized Zr-based superhydrophobic thin films on Al substrate have been properly investigated.

2 EXPERIMENTAL DETAILS

One by two inches AA6061 aluminum substrates with the chemical composition of Al 97.9 wt.%, Mg 1.08 wt.%, Si 0.63 wt.%, Mn 0.52 wt.%, Cu 0.32 wt.%, Fe 0.17 wt.%, Ti 0.02 wt.%, and V 0.01 wt.% were degreased in ultrasonic bath using soap water for 30 min, and then cleaned with deionized water and ethanol. A mixture of Zirconium (IV) propoxide (ZrO_x) and ethanolic stearic acid (SA) solution was used as an electrolyte and two cleaned Al substrates separated at a distance of 2 cm were used as electrodes. The electrodeposition time was fixed at 10 minutes under a DC potential of 10 V. Electrolyte with different concentrations were prepared by varying the Zr/SA molar ratios. After the electro-deposition process, the samples were removed carefully from the chemical bath and dried the substrate at 70°C for 10 h in an air environment. The surface morphology of the fabricated thin films on Al substrate was characterized using a scanning electron microscope (SEM). The surface chemical composition was studied using Fourier-transform infrared spectroscopy (ATR-FTIR) and energy dispersive X-ray spectroscopy (EDS). The wetting properties of the fabricated thin films on Al substrates were carried out by measuring the static contact angle using a first ten-angstrom contact angle goniometer. A three electrodes set-up, consisting of a platinum mesh (counter electrode), a silver/silver-chloride (Ag-AgCl) (reference electrode), and the Al samples (working electrodes) was employed for potentiodynamic polarization studies. The polar-

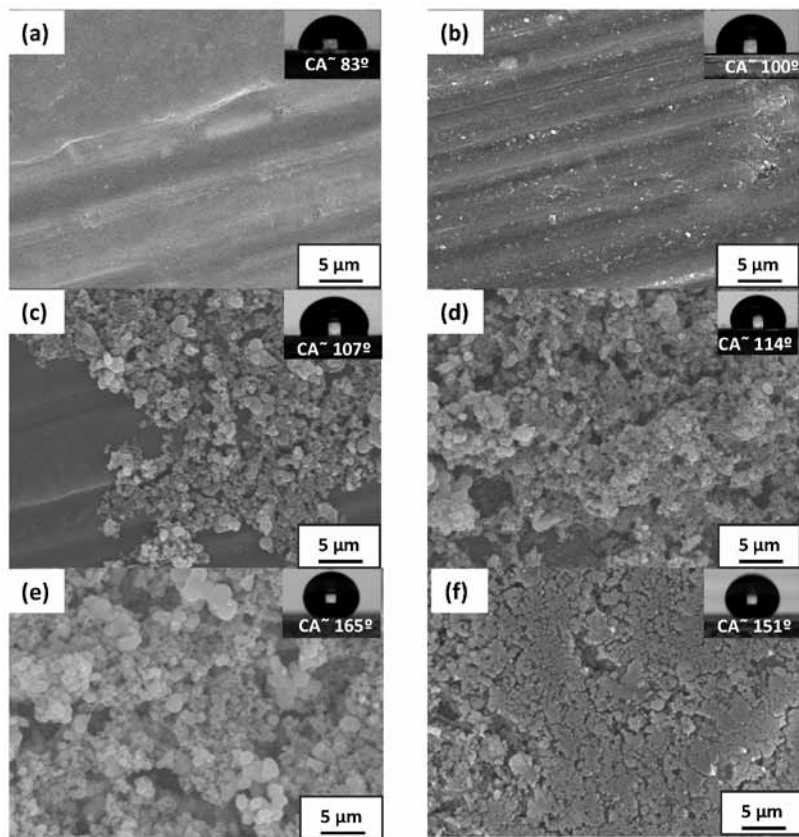


FIGURE 1

SEM images of (a) as-received Al substrate, and ZrSA thin films electrodeposited on the Al substrates with the Zr/SA molar ratio of (b) 0, (C) 1, (d) 2, (e) 4, and (f) 8, with the insets represent the corresponding CA values.

ization curves were recorded at a sweep rate of 2 mV/s in a range of -250 mV to 1000 mV with respect to open circuit potential (OCP). The frequency range of electrochemical impedance spectroscopy (EIS) study was fixed between 10^{-2} and 10^5 Hz with an amplitude of 20 mV with respect to OCP. All the electrochemical experiments were carried out in 3.5 wt.% NaCl solution (pH of 5.8) to simulate seawater.

3 RESULTS AND DISCUSSION

Figure 1(a) shows the SEM image of the as-received Al substrate, which had a surface roughness of $0.41 \pm 0.04 \mu\text{m}$ and a water contact angle (CA) of $83 \pm 2^\circ$

(shown in the inset of Figure 1(a)). The as-received Al substrate exhibits parallel streaks which are resulting from the mechanical rolling operations [27]. Figure 1(b) shows the surface morphology of the sample prepared by electro-deposition process in the ethanolic stearic acid bath. The CA of this sample was found to be increased to $100\pm 4^\circ$ and this increase of CA results from the presence of the low surface energy radicals $-\text{CH}_2$ and $-\text{CH}_3$ on the metallic substrate [28]. Interestingly, the electro-deposition process performed in the electrolyte of the Zr/SA molar ratio of 1 leads to the formation of micro-nano structures on the Al substrate as shown in Figure 1(c). The deposition of these micro-nano structures on the Al substrates under the effect of the electric field increases the CA of the surface to $107\pm 6^\circ$. Further, when the Zr/SA molar ratio increased to a value of 2, as expected, more ZrSA compounds are formed leading to more amounts of deposits and higher coverage of micro-nano structures on the Al surface. This surface exhibits a CA of $114\pm 9^\circ$ as shown in the inset of Figure 1(d). On the other hand, Figure 1(e) shows the deposition of ZrSA compounds in complete coverage on the Al surface when the Zr/SA molar ratio in the electrolyte reached the value of 4. The morphology of the deposited thin film on the surface exhibits micro-nanostructures. The combination of micro-nanorough compounds and low surface energy stearate radicals transforms the Al surface to a superhydrophobic surface with the highest CA value of $165\pm 3^\circ$. Further increase of Zr/SA molar ratio to 8, decreases the CA of the coated Al substrate to a value of $151\pm 4^\circ$ and is shown in Figure 1(f). The decrease in the CA could be explained by the increase of the deposited cluster size, which leads to more micro-sized morphology. These results are supported by the roughness measurements discussed later in Figure 4(b).

Figure 2 shows the EDS of the as-received Al substrate and the fabricated thin films with different Zr/SA molar ratios. The results of the elemental composition analysis are presented in Table 1. It can be seen from the EDS graphs that all the thin films contain the elements of C and O with their respective $K\alpha$ peaks at 0.27 and 0.52 KeV. While the $L\alpha$ peak of Zr is observed at 2.04 KeV for the thin films fabricated from the Zr/SA molar ratios of 1, 2, 4 and 8. It must be mentioned that the peak at 1.48 KeV is related to the $K\alpha$ of Al resulted from the metallic substrate. The EDS for Zr/SA molar ratios of 4 and 8 show no peak related to Al, which is resulted from the higher thickness of the deposited thin films on the Al substrate as shown in Figure 4(a).

The variation of the atomic percentage of zirconium with the Zr/SA molar ratio was illustrated in Figure 3(a). It can be seen from the figure that the increase of Zr/SA molar ratio in the electrolyte leads to the increase of zirconium atomic percentage in the electrodeposited thin films. Furthermore, the variation of the atomic percentage of O/C with the Zr/SA molar ratio has been presented in Figure 3(b). The atomic ratio of O/C is found to increase with the increase of the Zr/SA molar ratio, which exhibits more zirconium oxide formation on the Al substrate.

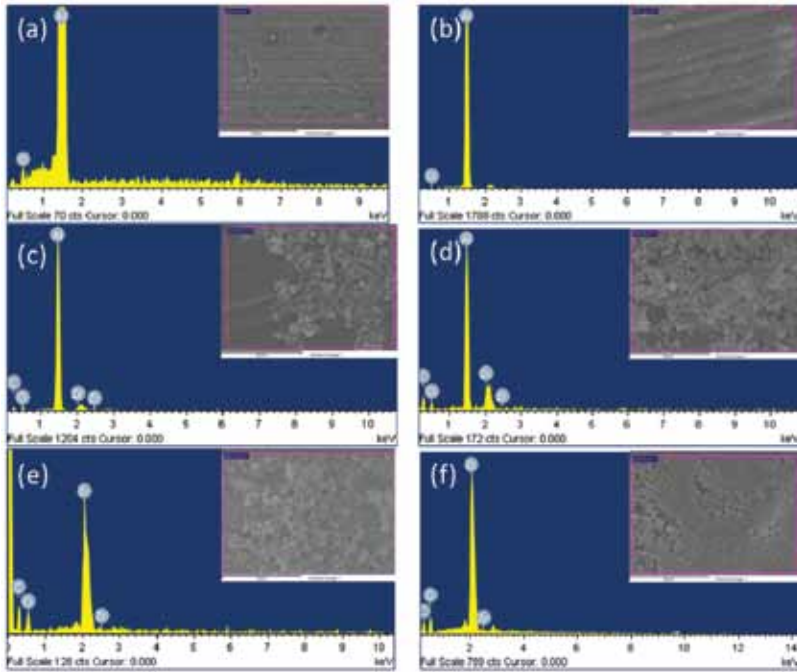


FIGURE 2

EDS spectra of (a) as-received Al substrate, and ZrSA thin films electrodeposited on the Al substrates with the Zr/SA molar ratio of (b) 0, (c) 1, (d) 2, (e) 4, and (f) 8. The insets of the images represent the corresponding SEM images.

TABLE 1

Elemental composition electrodeposited ZrSA thin films on Al substrate with different Zr/SA molar ratios.

Zr/SA molar ratio	Thin films chemical composition (at. %)		
	C	O	Zr
0	85.75	14.24	0
1	87.53	11.58	0.88
2	78.07	18.71	3.21
4	64.99	27.87	7.15
8	53.36	32.13	14.51

Figure 4(a) illustrates the variation of the thickness of the fabricated thin films with Zr/SA molar ratio. With the increase of Zr/SA molar ratio, the thickness of the deposited thin films increases and this could be explained by the deposition of more amount of ZrSA and zirconium oxide compounds on

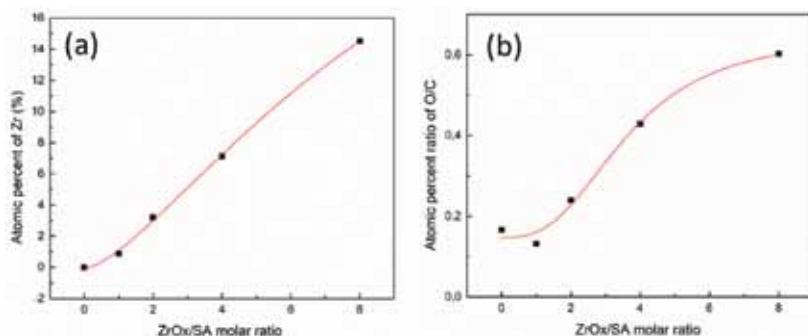


FIGURE 3 The evolution of the atomic percentage of (a) Zr and (b) the atomic percentage ratio of O/C in the fabricated thin films with the Zr/SA ratios of 0, 1, 2, 4 and 8.

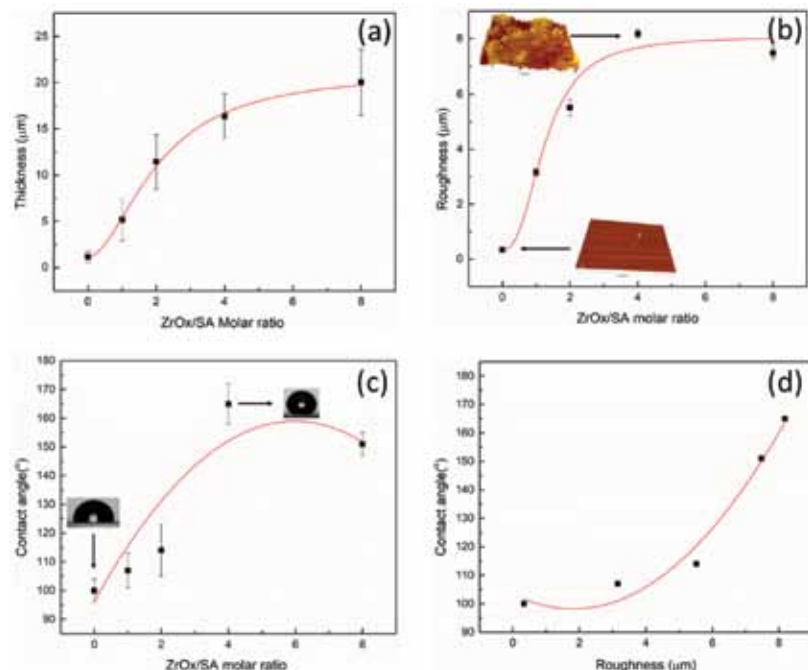


FIGURE 4 (a) The evolution of the thickness (b) the roughness (c) and the CA of the fabricated thin films with the Zr/SA molar ratios of 0, 1, 2, 4 and 8. (d) represents the variation of the CA with the roughness of the fabricated thin films.

Al substrate under DC voltage. Furthermore, Figure 4(b) represents the variation of the roughness of the ZrSA thin films. The roughness of the thin film fabricated from the Zr/SA molar ratio of 0 (only SA) is found to be 0.44 ± 0.02

μm compared to $0.41\pm 0.04 \mu\text{m}$ for as-received Al substrate. Similar roughness values have been reported previously in the literature [29]. Interestingly, the roughness of the thin film fabricated from Zr/SA molar ratio 1 found to be increased to $3.12\pm 0.16\mu\text{m}$, this increase in the roughness is related to the deposition of ZrSA compounds with the micro-nano rough structures on the Al surface. Furthermore, the roughness of the fabricated thin films reaches a maximum value of $8.18\pm 0.17 \mu\text{m}$ with the Zr/SA molar ratio of 4, which is resulted from the total coverage area of the thin film as shown in the SEM image. A slight decrease of the roughness was observed with the Zr/SA molar ratio of 8, which could be resulted from the agglomeration of deposited compounds (ZrSA and ZrOx) on the Al surface.

Figure 4(c) shows the evolution of the CA of the fabricated thin films with the Zr/SA molar ratios of 0, 1, 2, 4, and 8. The CA reaches a maximum value of $165\pm 3^\circ$ at the molar ratio of 4, this could be explained by the combination of high surface roughness and low surface energy of the fabricated thin film deposited on Al substrate. Further, a slight decrease of the CA was measured at the Zr/SA molar ratio of 8, which could be related to the decrease of the roughness of the thin film compared to the thin film fabricated from the Zr/SA molar ratio of 4. For better understanding, the variation of the CA of the ZrSA thin films with their roughness was illustrated in Figure 4(d), and the results show that the CA is increasing with the increase of the roughness of the fabricated thin films.

The chemical composition of the ZrSA thin films on Al substrates was studied using ATR-FTIR analysis in the wavelength range of $450\text{-}4000 \text{ cm}^{-1}$. Figure 5 shows the spectra of the electrodeposited thin films with the Zr/SA molar ratios of 1, 2, 4 and 8. At the high-frequency region, the peaks of the relevant alkyl chain of $-\text{CH}_2$ and $-\text{CH}_3$ can be seen at the wavelength values of 2852 , 2921 and 2961 cm^{-1} , respectively [2,30]. Due to the presence of these alkyl groups, the surface energy of the electrodeposited ZrSA thin films decreases [31].

Furthermore, the mid-frequency region exhibits a peak at 1542 cm^{-1} , this peak is related to the formation of COOZr bond in the fabricated thin films [32]. Similarly, the bond formation of COOCo and COOAl at the respective positions of 1550 and 1586 cm^{-1} were reported in our previous works [14,17]. The shift of the COOZr bond towards lower wavenumber compared to COOCo and COOAl bonds is due to the higher atomic number of Zr compared to Co and Al [14]. Another peak around 616 cm^{-1} is observed and that is assigned to Zr-O stretching mode, indicating the presence of zirconium oxide in the chemical composition of the fabricated thin films [33]. The ATR-FTIR spectra of the thin film fabricated from Zr/SA=0 (only SA) and ZrOx (Without SA) separately were presented in Figure 5, and no clear peak was observed.

The peak area analysis of the chemical bonds of $-\text{CH}_3$, $-\text{CH}_2$, and Zr-O was performed for the FTIR spectra of the electrodeposited thin films fabricated from the Zr/SA molar ratio of 0, 1, 2, 4 and 8, and the results are presented in Figure

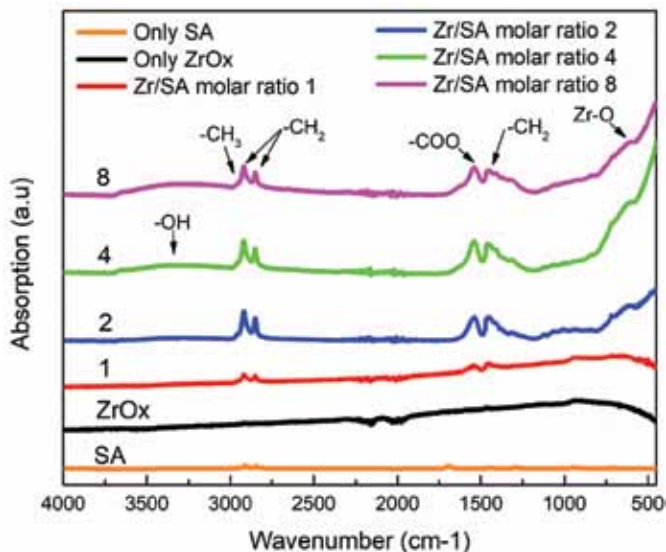


FIGURE 5

ATR-FTIR spectra of superhydrophobic ZrSA thin films with different Zr/SA molar ratios (1, 2, 4 and 8), stearic acid (Only SA), and ZrO_x (without SA) on the Al substrates.

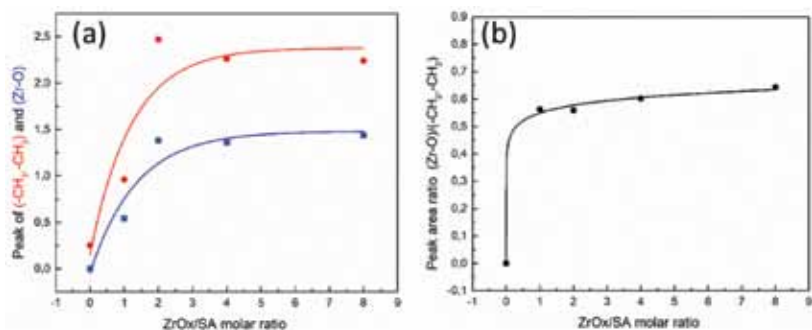


FIGURE 6

The variation of the peak area of (a) $-CH_3$ and CH_2 peaks (red squares), and Zr-O peak (Blue squares), (b) the ratio of peak area of $-CH_3$, CH_2 and Zr-O.

6(a). The peak area of CH_2 and CH_3 increases with the increase of Zr/SA molar ratio and reaches to a value of 2.28 for the ratio of 4, which indicates that more ZrSA compound is deposited uniformly on the Al surface. A slight decrease of the area was observed for the Zr/SA molar ratio of 8, which could be explained by the decrease in the SA molecules in the electrochemical bath and consequently less deposition on the substrate. On the other hand, the peak area of Zr-O increases gradually with the increase of the Zr/SA molar ratio in the electrolyte, which

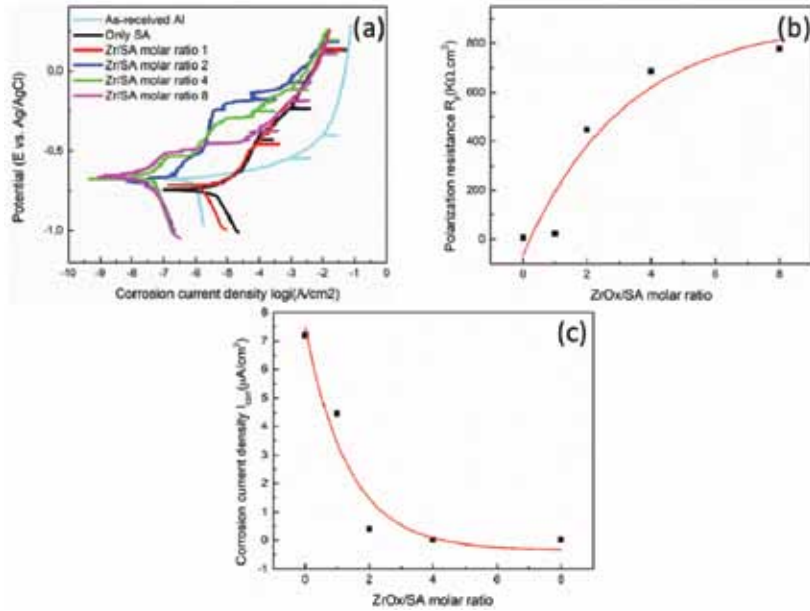


FIGURE 7

(a) Potentiodynamic polarization curves of as-received Al substrate and ZrSA thin films fabricated by electrodeposition process with the Zr/SA molar ratio of 0, 1, 2, 4, and 8. The variation of the (b) polarization resistance R_p and the (c) corrosion current density I_{corr} with the Zr/SA molar ratio.

shows that more zirconium oxide is deposited on the Al substrate under the application of DC voltage of 10 V. Furthermore, Figure 6(b) represents the variation of the peak area ratio of $(Zr-O)/(-CH_3, -CH_2)$. The peak area ratio reaches a maximum value at the Zr/SA molar ratio of 8, indicating that more zirconium oxide (hydrophilic in nature) is deposited on the Al surface, which correlates the decrease of the CA to the value of 151° for this sample.

Figure 7(a) shows the potentiodynamic polarization curves (Tafel curves) of the as-received Al substrate and ZrSA thin films deposited substrate. The corrosion potential (E_{corr}) and the corrosion current density (I_{corr}) were determined from the extrapolation of the anodic and cathodic Tafel slopes, while the polarization resistance, R_p , was calculated using the Stern-Geary equation, given by the following formula:

$$R_p = \frac{\beta_a \beta_c}{2.3 I_{corr} (\beta_a + \beta_c)} \quad (1)$$

Where, β_a and β_c are the anodic and cathodic Tafel slopes, respectively. The polarization resistance and the corrosion current density of the as-

received Al substrate were found to be $22 \pm 2 \text{ k}\Omega \cdot \text{cm}^2$ and $3.6 \pm 1 \text{ }\mu\text{A}/\text{cm}^2$, respectively. These results are comparable with the existing literature on the corrosion studies of Al [17]. Furthermore, the R_p and I_{corr} for the thin film of SA ($\text{Zr}/\text{SA} = 0$) on the Al substrate were found to be $6 \pm 22.2 \text{ k}\Omega \cdot \text{cm}^2$ and $7.2 \pm 0.27 \text{ }\mu\text{A}/\text{cm}^2$, respectively. This decrease in the anticorrosion property could be due to the dissolution of the protective oxide layer under the effect of SA. Moreover, a similar tendency was observed for the thin film fabricated from the Zr/SA molar ratio of 1. In this case, the R_p and I_{corr} were found to be $22 \pm 9 \text{ k}\Omega \cdot \text{cm}^2$ and $4.46 \pm 2 \text{ }\mu\text{A}/\text{cm}^2$, respectively. Further increase of Zr/SA molar ratio to 2 in the process, a larger R_p of $449 \pm 36 \text{ k}\Omega \cdot \text{cm}^2$ and a lower I_{corr} of $0.41 \pm 0.05 \text{ }\mu\text{A}/\text{cm}^2$ was observed. This can be correlated by the formation of a uniform ZrSA thin film on the Al substrate as shown in the SEM image (Figure 1(d)). With a further increase in the Zr/SA molar ratio to 4, the R_p value was increased to $686 \pm 178 \text{ k}\Omega \cdot \text{cm}^2$ and I_{corr} value was found to decrease $0.028 \pm 0.01 \text{ }\mu\text{A}/\text{cm}^2$ for the ZrSA film coated Al substrate. This coating with excellent anticorrosion properties is also associated with superhydrophobic properties. It was reported that the air trapped in the nanopores of superhydrophobic surfaces acts as a barrier and prevents the penetration of the corrosive ions to the Al substrate [34]. The R_p value increases to a maximum value of $778 \pm 102 \text{ k}\Omega \cdot \text{cm}^2$ for the ZrSA thin film fabricated from the Zr/SA molar ratio of 8, while the corresponding I_{corr} was found to be $0.02 \pm 0.01 \text{ }\mu\text{A}/\text{cm}^2$. The obtained R_p of this sample is 35 times higher than that obtained for the as-received Al substrate.

The corrosion parameters of the as-received Al substrate and the ZrSA thin film coated substrate are summarized in Table 2. The variations of R_p and I_{corr} with the Zr/SA molar ratio were illustrated in Figure 7(b) and Figure 7(c), respectively.

TABLE 2

The corrosion parameters and contact angle of as-received Al substrate and fabricated ZrSA thin films on Al substrate with the Zr-SA molar ratios of 0, 1, 2, 4 and 8.

Substrate	Corrosion potential E_{corr} (mV)	Corrosion current	Polarization	CA ($^\circ$)
		density I_{corr} ($\mu\text{A}/\text{cm}^2$)	resistance R_p ($\text{k}\Omega \cdot \text{cm}^2$)	
As-received Al	-610 ± 10	3.6 ± 1	22 ± 2	83 ± 2
Zr/SA=0(Only SA)	-710 ± 41	7.2 ± 0.27	6 ± 22	100 ± 4
Zr/SA=1	-737 ± 14	4.46 ± 2	22 ± 9	107 ± 6
Zr/SA=2	-696 ± 34	0.41 ± 0.05	449 ± 36	114 ± 9
Zr/SA=4	-683 ± 34	0.028 ± 0.01	686 ± 178	165 ± 3
Zr/SA=8	-704 ± 31	0.02 ± 0.01	778 ± 102	151 ± 4

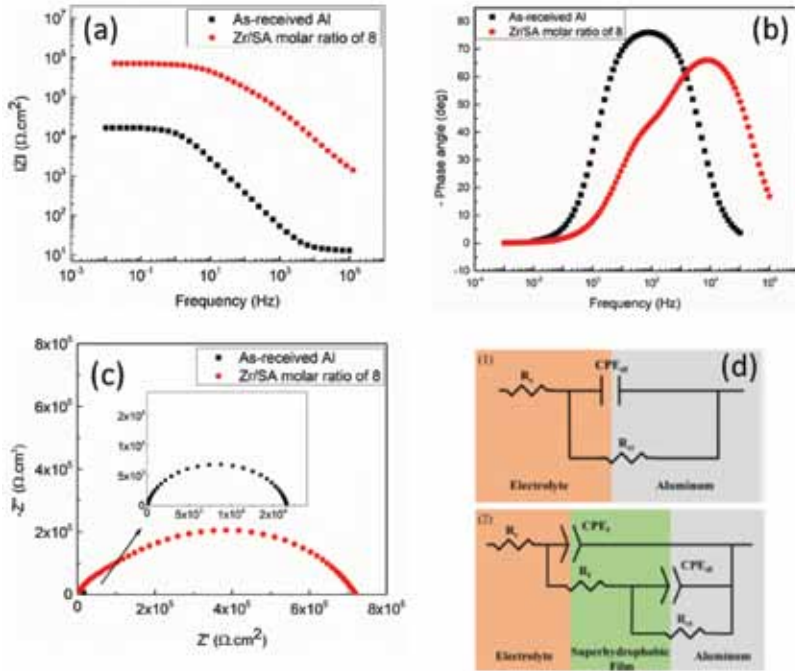


FIGURE 8

EIS measurements for the ZrSA thin films fabricated using the Zr/SA molar ratio of 8 and the as-received Al substrate. (a) The Nyquist plot, (b) Bode modulus, (c) Bode phase and (d) equivalent circuit of (d1) as-received Al substrate and (d2) superhydrophobic thin film.

As a complementary electrochemical technique, the electrochemical impedance spectroscopy (EIS) was used to evaluate the corrosion resistance properties of the fabricated thin films deposited on Al substrates. Figure 8(a) shows the Bode plot of the as-received Al substrate and the ZrSA superhydrophobic thin film fabricated from the Zr/SA molar ratio of 8. This plot presents the modulus of the impedance $|Z|$ as a function of the frequency. At a high frequency of 1×10^4 Hz, the $|Z|$ value of the as-received Al substrate and the ZrSA superhydrophobic thin film was found to be $21 \Omega \cdot \text{cm}^2$ and $8230 \Omega \cdot \text{cm}^2$, respectively. Similarly, at a low frequency of 1 Hz, the $|Z|$ value for the as-received Al and the ZrSA superhydrophobic thin film was found to be $25 \text{ k}\Omega \cdot \text{cm}^2$ and $578 \text{ k}\Omega \cdot \text{cm}^2$, respectively. In the whole frequency range, the superhydrophobic thin film exhibited higher impedance compared to the as-received Al substrate. It has to mention that larger impedance values at lower frequencies are generally related to better corrosion protection [35,36].

Furthermore, in Figure 8(b), the Bode phase plot of the ZrSA superhydrophobic thin film on Al substrate show two peaks corresponding to two differ-

TABLE 3

Impedance parameters of the electrical equivalent circuits (EEC) and fitted EIS data of solution resistance (Rs), film resistance (Rf), charge transfer resistance (Rct), constant phase element (CPE).

	R_s ($\Omega \cdot \text{cm}^2$)	CPE_f		R_f ($\text{k}\Omega \cdot \text{cm}^2$)		CPE_{dl}	
		Y_f ($\Omega^{-1} \cdot \text{s}^n \cdot \text{cm}^{-2}$)	n_f	n_f	Y_f ($\Omega^{-1} \cdot \text{s}^n \cdot \text{cm}^{-2}$)	n_f	R_{ct} ($\text{k}\Omega \cdot \text{cm}^2$)
Aluminum substrate	22	-	-	-	2.3×10^{-6}	0.9	37
Superhydrophobic thin film	597	1.6×10^{-8}	0.8	1.6×10^2	8.6×10^{-8}	0.6	552

ent time constants. The time constant situated at the frequency of 10^4 Hz is related to thin film capacitance, and the time constant at a low frequency of 60 Hz is assigned to the capacitance of the double layer near the metallic substrate. This peak has been shifted toward lower frequency compared to as-received Al (90 Hz), indicating better anticorrosion properties with the fabrication of superhydrophobic thin film on Al.

Figure 8(c) shows the Nyquist plots of the ZrSA thin films on Al substrate and the as-received Al substrate, which represents the impedance imaginary component Z'' as a function of the real component Z' . The Nyquist plot of the as-received Al is composed of a small semi-circle with a diameter of $37 \text{ k}\Omega \cdot \text{cm}^2$, while the superhydrophobic thin film shows a large semi-circle with a diameter of $552 \text{ k}\Omega \cdot \text{cm}^2$. It has to mention that the diameter of the semi-circle in the Nyquist plots is related to the charge transfer resistance (R_{ct}), which is associated with the corrosion properties of the sample. A high R_{ct} value provides excellent anticorrosion properties for the superhydrophobic thin film. Figure 8(d1) and Figure 8(d2) represents the electrical equivalent circuits (EECs) of the as-received Al and the ZrSA superhydrophobic thin film. The fitted results obtained using the EECs are summarized in Table 3.

The inhibition efficiency (η) of ZrSA superhydrophobic thin film was evaluated using the following equation:

$$\eta(\%) = \frac{R_{ct} - R_{ct0}}{R_{ct}} \times 100 \tag{2}$$

Where, R_{ct} is the charge transfer resistance of ZrSA superhydrophobic thin film, and R_{ct0} represents the charge transfer resistance of the Al substrate. In this case, the inhibition efficiency η (%) of the superhydrophobic thin film is 93 % by taking the values of R_{ct} and R_{ct0} of $552 \text{ k}\Omega$ and $37 \text{ k}\Omega \cdot \text{cm}^2$ respectively. This result indicates that ZrSA thin film exhibits excellent anticorrosion properties.

4 CONCLUSIONS

In the current study, Zr-based superhydrophobic thin films were successfully fabricated on aluminum substrates using the electrodeposition process. The SEM images of the Zr-based thin film coated substrate show the presence of micro-nano patterned surface. The ATR-FTIR confirms the presence of low surface energy compounds on the ZrSA thin film coated substrates. The synthesized Zr-based superhydrophobic thin films provide much higher water contact angle and polarization resistance as compare to as-received aluminum substrate. The maximum corrosion protection efficiency of 93 % was achieved for Zr-based superhydrophobic thin films, which is beneficial to expand the application of Al and its alloys in a variety of practical fields.

5 ACKNOWLEDGMENTS

This project was supported by Natural Science and Engineering Research Council of Canada (NSERC), University of Quebec at Chicoutimi (UQAC) and Aluminum Research Centre (REGAL). Redouane thanks REGAL for the support of graduate research fellowship.

REFERENCES

- [1] Lee D.J., Kim H.M., Song Y.S. and Youn J.R. Water Droplet Bouncing and Superhydrophobicity Induced by Multiscale Hierarchical Nanostructures. *ACS Nano* **6** (2012), 7656–7664.
- [2] Chen Z., Hao L., Chen A., Song Q. and Chen C. A rapid one-step process for fabrication of superhydrophobic surface by electrodeposition method. *Electrochimica Acta* **59** (2012), 168–171.
- [3] Alonso Frank M., Boccaccini A.R. and Virtanen S. A facile and scalable method to produce superhydrophobic stainless steel surface. *Applied Surface Science* **311** (2014), 753–757.
- [4] Tong W., Xiong D., Wang N., Yan C. and Tian T. Green and timesaving fabrication of a superhydrophobic surface and its application to anti-icing, self-cleaning and oil-water separation. *Surface and Coatings Technology* **352** (2018), 609–618.
- [5] Kuang J., Ba Z., Li Z., Jia Y. and Wang Z. Fabrication of a superhydrophobic Mg-Mn layered double hydroxides coating on pure magnesium and its corrosion resistance. *Surface and Coatings Technology* **361** (2019), 75–82.
- [6] Li H., Yu S., Hu J. and Yin X. Modifier-free fabrication of durable superhydrophobic electrodeposited Cu-Zn coating on steel substrate with self-cleaning, anti-corrosion and anti-scaling properties. *Applied Surface Science* **481** (2019), 872–882.
- [7] Rius-Ayra O., Castellote-Alvarez R., Escobar A.M. and Llorca-Isern N. Robust and superhydrophobic coating highly resistant to wear and efficient in water/oil separation. *Surface and Coatings Technology* **364** (2019), 330–340.
- [8] Zhao Q., Tang T. and Wang F. Fabrication of Superhydrophobic AA5052 Aluminum Alloy Surface with Improved Corrosion Resistance and Self Cleaning Property. *Coatings* **8** (2018), 390.

- [9] Donahue C.J. and Exline J.A. Anodizing and coloring aluminum alloys. *Journal of Chemical Education* **91** (2014), 711–715.
- [10] Li Z., Li N., Wang D., Ouyang D. and Liu L. Low temperature deformation behavior of an electromagnetically bulged 5052 aluminum alloy. *Scientific Reports* **6** (2016), 29973.
- [11] Liang M., Melchers R. and Chaves I. Corrosion and pitting of 6060 series aluminium after 2 years exposure in seawater splash, tidal and immersion zones. *Corrosion Science* **40** (2018), 286–296.
- [12] Hintze P.E. and Calle L.M. Electrochemical properties and corrosion protection of organosilane self-assembled monolayers on aluminum 2024-T3. *Electrochimica Acta* **51** (2006), 1761–1766.
- [13] Barkhudarov P.M., Shah P.B., Watkins E.B., Doshi D.A., Brinker C.J., and Majewski J. Corrosion inhibition using superhydrophobic films. *Corrosion Science* **50** (2008), 897–902.
- [14] Huang Y., Sarkar D.K. and Chen X.-G. Superhydrophobic aluminum alloy surfaces prepared by chemical etching process and their corrosion resistance properties. *Applied Surface Science* **356** (2015), 1012–1024.
- [15] Li X., Zhang Q., Guo Z., Shi T., Yu J., Tang M. and Huang X. Fabrication of superhydrophobic surface with improved corrosion inhibition on 6061 aluminum alloy substrate. *Applied Surface Science* **342** (2015), 76–83.
- [16] Alawajji R.A., Kannarpady G.K. and Biris A.S., Fabrication of transparent superhydrophobic polytetrafluoroethylene coating. *Applied Surface Science* **444** (2018), 208–215.
- [17] Xiong J., Sarkar D.K. and Chen X.-G. Superhydrophobic honeycomb-like cobalt stearate thin films on aluminum with excellent anti-corrosion properties. *Applied Surface Science* **407** (2017), 361–370.
- [18] Huang Y., Sarkar D.K. and Chen X.-G. Superhydrophobic nanostructured ZnO thin films on aluminum alloy substrates by electrophoretic deposition process. *Applied Surface Science* **327** (2015), 327–334.
- [19] Xu N., Sarkar D.K., Chen X.-G., Zhang H. and Tong W. Superhydrophobic copper stearate/copper oxide thin films by a simple one-step electrochemical process and their corrosion resistance properties. *RSC Advances* **6** (2016), 35466–35478.
- [20] Xu N., Sarkar D.K., Chen X.-G. and Tong W.P. Corrosion performance of superhydrophobic nickel stearate/nickel hydroxide thin films on aluminum alloy by a simple one-step electrodeposition process. *Surface and Coatings Technology* **302** (2016), 173–184.
- [21] Brassard J.D., Sarkar D.K., Perron J., Audibert-Hayet A. and Melot D. Nano-micro structured superhydrophobic zinc coating on steel for prevention of corrosion and ice adhesion. *Journal of Colloid and Interface Science* **447** (2015), 240–247.
- [22] Singh A.K. and Singh J.K. Fabrication of zirconia based durable superhydrophobic-superoleophilic fabrics using non fluorinated materials for oil-water separation and water purification. *RSC Advances* **6** (2016), 103632–103640.
- [23] Fan Y., He Y., Luo P., Chen X., Yu Z. and Li M. Facile way in building superhydrophobic zirconium surface for controllable water-oil separation. *Materials Letters* **188** (2017), 115–118.
- [24] Das I. and De G. Zirconia based superhydrophobic coatings on cotton fabrics exhibiting excellent durability for versatile use. *Scientific Reports* **5** (2016), 18503.
- [25] Li H., Liang K., Mei L., Gu S. and Wang S. Corrosion protection of mild steel by zirconia sol-gel coatings. *Journal of Materials Science Letters* **20** (2001), 1081–1083.
- [26] Li Q.P., Yan Z.Q., Xu Q., Zhang B., Sun S., Liu J.G. and Yan C.W. A high-performance Ti-Zr Based Chromium-Free Conversion Coating on 2024 Aluminum Alloy. *International Journal of Electrochemical Science* **1112** (2016), 10675–1068939.
- [27] Gheyfani S., Liang Y., Jing Y., Xu J.Q. and Yao Y. Chromate conversion coated aluminium as a light-weight and corrosion-resistant current collector for aqueous lithium-ion batteries. *Journal of Materials Chemistry A* **4** (2016), 395–399.
- [28] Tsiouklis J., Graham P., Eaton P.J., Smith J.R., Nevell T.G., Smart J.D. and Ewen R.J., Poly(perfluoroalkyl methacrylate) Film Structures: Surface Organization Phenomena,

- Surface Energy Determinations, and Force of Adhesion Measurements. *Macromolecules* **33** (2000), 8460–8465.
- [29] Kadlečková M., Minařík A., Smolka P., Mráček A., Wrzecionko E., Novák L., Musilová L. and Gajdošík R. Preparation of Textured Surfaces on Aluminum-Alloy Substrates. *Materials* **12** (2018), 109.
- [30] Fonder G., Laffineur F., Delhalle J. and Mekhalif Z. Alkanethiol-oxidized copper interface: The critical influence of concentration. *Journal of Colloid and Interface Science* **326** (2008), 333–338.
- [31] Tan J., Hao J., An Z. and Liu C. Simple Fabrication of Superhydrophobic Nickel Surface on Steel Substrate via Electrodeposition. *International Journal of Electrochemical Science* **12** (2017), 40–49.
- [32] Li B., Mou H., Li Y. and Ni Y. Synthesis and thermal decomposition behavior of zircoaluminate coupling agents. *Industrial and Engineering Chemistry Research* **52** (2013), 11980–11987.
- [33] Li W., Liu X., Huang A. and Chu P.K. Structure and properties of zirconia (ZrO₂) films fabricated by plasma-assisted cathodic arc deposition. *Journal of Physics D: Applied Physics* **40** (2007), 2293–2299.
- [34] Zhang B., Li J., Zhao X., Hu X., Yang L., Wang N., Li Y. and Hou B. Biomimetic one step fabrication of manganese stearate superhydrophobic surface as an efficient barrier against marine corrosion and *Chlorella vulgaris*-induced biofouling. *The Chemical Engineering Journal* **306** (2016), 441–451.
- [35] Twite R.L. and Bierwagen G.P. Review of alternatives to chromate for corrosion protection of aluminum aerospace alloys, *Progress in Organic Coatings* **33** (1998), 91–100.
- [36] Denissen P.J. and Garcia S.J. Reducing subjectivity in EIS interpretation of corrosion and corrosion inhibition processes by in-situ optical analysis. *Electrochimica Acta* **293** (2019), 514–524.